

# Dynamics of Charged Polyionic Liquids

Thesis by  
Christopher J. Stewart

In Partial Fulfillment of the Requirements for the  
Degree of  
Master of Science in Chemical Engineering

The Caltech logo is displayed in a bold, orange, sans-serif font. The letters are thick and closely spaced, with a clean, modern aesthetic.

CALIFORNIA INSTITUTE OF TECHNOLOGY  
Pasadena, California

2025  
Submitted May 22, 2025

© 2025

Christopher J. Stewart  
ORCID: 0009-0001-0280-2336

All rights reserved except where otherwise noted

## ACKNOWLEDGEMENTS

I want to begin by expressing my deepest gratitude to Professor Wang for his unwavering willingness to work with me, his constant mentorship, and his dedicated commitment to my success. He has been instrumental in clearing a path for me to pursue a terminal master's degree, guiding me every step of the way as I transformed from soldier to student. I could not have asked for a better Research Advisor.

To the entire Wang group, thank you for welcoming me into your midst, for your mentorship, expertise, and friendship. The two years I have spent at Caltech have been a profoundly broadening experience, one that would have been impossible without your support.

I would also like to extend my heartfelt thanks to the Caltech Chemical Engineering program and everyone involved in opening the door for me to pursue this academic journey. Thank you Allison Kinnard and Mike Vicic for the support and assistance navigating the last two years.

To the United States Army, and specifically the Chemistry and Life Science department at the United States Military Academy, thank you for the trust and opportunity to pursue a master's degree mid-career. I am eager to bring the knowledge and training I have gained back to our Cadets and their intellectual pursuits.

Finally, I would like to express my deepest appreciation to my wife, Laura, for following me on this journey, for her steadfastness, and for her continued support as I pursue my passions. A special thank you to my parents for their love and support while we have been in Southern California.

## ABSTRACT

Polymerized ionic liquids (PILs) exhibit complex ion transport dynamics that are central to advancing technology in energy storage and efficient energy conversion. In this work, we probe the behavior of charged polymer systems in the solvent-free limit using a coarse-grained Gaussian core model that explicitly incorporates long-range electrostatic interactions. Our simulations span a wide range of chain lengths, from monomeric units to highly entangled polymers, revealing how both intrachain and interchain interactions govern key properties such as the radius of gyration, relaxation time, and diffusivity. Notably, charged polymers adhere to classical reptation scaling, indicating that electrostatic forces do not inhibit standard polymer melt scaling behavior. We quantify these effects by evaluating both the Onsager transport coefficients and the direct drift response under applied electric fields, thereby linking molecular trajectories to macroscopic ion conductivity.

Our findings show that as the chain length increases, the motion of polymerized ions becomes increasingly correlated, a trend that stabilizes ion conductivity despite decreasing diffusivity. This study demonstrates that the complex interplay between correlated motion and cooperative chain dynamics results in a relatively stable conductivity that increases over short chain length, plateaus in the transition regime, before decreasing in the fully entangled regime — contrary to idealized predictions based solely on diffusivity. By explicitly modeling the microscopic interactions and accounting for both hydrodynamic and electrostatic effects, we provide a physically grounded framework that captures the emergent behavior of these charged systems. In doing so, our work offers a robust platform for the rational design of next-generation PIL electrolytes, distinguishing itself from phenomenological models through clear, simulation-based insights.

## TABLE OF CONTENTS

Acknowledgements . . . . .	iii
Abstract . . . . .	iv
Table of Contents . . . . .	v
List of Illustrations . . . . .	vi
Chapter I: Introduction/Polyionic Liquids . . . . .	1
Chapter II: Dynamics of Gaussian Core Modeled Polyionic Liquid Systems . . . . .	7
2.1 Methodology . . . . .	8
2.2 Results and Discussion . . . . .	9
2.3 Conclusion . . . . .	24
Appendix A: Gaussian Core Model . . . . .	29
A.1 Model and Parameterization . . . . .	29
A.2 Applied Electric Field . . . . .	31
A.3 Conclusion . . . . .	32
Appendix B: Onsager Transport Coefficient Fitting . . . . .	34
B.1 Mean Squared Displacement and Diffusivity . . . . .	34
B.2 Onsager Coefficient . . . . .	36

## LIST OF ILLUSTRATIONS

<i>Number</i>	<i>Page</i>
1.1 Example coarse graining of ionic liquid monomer [BMIM+] [24] into a hard sphere . . . . .	3
2.1 Example system snapshot for a polyanion (blue) and cation (red) system with chain length, $N = 50$ - visualized using Ovito [1] . . . . .	7
2.2 Radius of gyration for polyanion and neutral system polymers as a function of the chain length, showing a scaling relationship of .52 for the charged system and .53 for the uncharged system [8] . . . . .	10
2.3 End to end autocorrelation function plotted against time for a range of chain lengths . . . . .	11
2.4 Plot of relaxation time vs. chain length for polyanions in our polymerized ionic liquid system compared to an identical uncharged system, showing scaling relationship of $\sim N^{3.00}$ in the fully entangled region. Note the scaling in the transition regime is $\sim N^{2.25}$ ( $25 < N < 100$ ) and $\tau$ here is the characteristic time scale defined in equation A.11 . . . . .	12
2.5 Diffusivity vs. chain length showing an unentangled scaling relationship of $N^{-1.08}$ system and a reptation scaling relationship of approximately $N^{-2.06}$ for our polyanion. Similarly, the uncharged system shows a scaling relationship of $N^{-.97}$ and $N^{-2.06}$ in the unentangled and entangled regimes respectively. . . . .	14
2.6 Center of mass diffusivity for the charged polyanion system compared to central bead diffusion, showing agreement between the two methods, even at our longer chain lengths . . . . .	15
2.7 Onsager transport coefficients for polyanion system. Note the $L_{++}$ and $L_{--}$ overlap near-perfectly and may not be distinguishable . . . . .	18
2.8 Illustration of correlated and anticorrelated anion/cation motion for our PIL system. 2.19 . . . . .	19
2.9 $L_{--}$ for both charged and uncharged system plotted against chain length for direct comparison. Note for both two component systems where all particles have the same mass, $L_{--}$ contains the same information as the other two Onsager Coefficients. . . . .	20

2.10	Ion conductivity calculated from Onsager transport coefficients for polyanion system . . . . .	21
2.11	Conductivity and Nernst-Einstein Conductivity vs. Chain Length . .	23
2.12	Example trajectory showing fitting data for drift velocity, $v_z$ , extraction from applied electric field . . . . .	24
2.13	Example plot of drift velocity $V_z$ versus electric field - notice the linear response as we increase the field strength and the clear intercept with the origin . . . . .	25
2.14	Plot of conductivity vs. chain length for applied electric field simulations . . . . .	25
A.1	Electric field graphic . . . . .	32
B.1	Example log-log mean squared displacement of charged polyanion system where diffusive slope = 1. Also displayed is linear scale of the same trajectory. . . . .	35
B.2	Example log-log mean squared displacement of uncharged polymer system where diffusive slope = 1. Note comparatively short time scale to enter diffusive regime when compared to polyanion system. .	35
B.3	Mean squared displacement, for cation and polyanions in our static system, varied over chain length. Diffusivity values were fit from the diffusive regime, where the log-log slope is 1 (dashed line). . . . .	36
B.4	"MSD" terms for the full $L_{ij}$ terms in the Onsager transport coefficient framework that were used to fit data with a reference slope of 1. Note, longer chained trajectories were run for longer periods of time to achieve full relaxation and ensure trajectories are in the diffusive regime. . . . .	37

*Chapter 1*

## INTRODUCTION/POLYIONIC LIQUIDS

Polymerized Ionic Liquids (PILs) have gained increasing research interest as charge-dense materials with wide applications including energy storage [1], separations membranes [2, 3], transistors [4], catalysis [5], and sensors [6]. PILs are composed of ionically charged monomer units and their corresponding counter-ions, and can exhibit liquid-like ionic conductivity at room temperature [7]. Particularly for energy storage applications, these materials are desirable due to their unique combination of high ionic conductivity, diffusivity, and relative durability compared to other energy storage materials, all maintained at standard operational temperatures [8]. Understanding how these critical dynamic properties scale with adjustable parameters like polymer chain length and composition is crucial for optimizing these materials for various applications.

While experimentalists have made significant strides in synthesizing, studying, and tuning polymerized ionic liquids, there remain substantial hurdles in examining these charge-dense systems [5]. In the solvent-free limit, high molecular weight or long-chained PILs exhibit relatively high glass transition temperatures compared to conventional experimental settings. Below this temperature, polymers exist in a glassy state where ion conductivity along with other transport properties are substantially decreased; reaching and maintaining temperatures above the glass transition temperature can be challenging from an experimental perspective [9]. Despite advances in synthesis techniques, creating and consistently characterizing polymerized ionic liquid systems remains a challenging area of research [10, 11]. PILs, like their uncharged polymer melt equivalents, exhibit a positive relationship between their chain length and glass transition temperature - where an increase in chain length necessarily leads to an increase in glass transition temperature [12–14]. Consequently, in long-chain polymers, the glass transition temperature plateaus at a prohibitively high value, preventing the polymer melt from remaining fluid at temperatures that are experimentally accessible. Even when these systems are experimentally accessible, decoupling the intrinsic effects of chain length from those induced by state transitions is challenging due to overlapping phase behavior and interdependent transport phenomena [15]. Additionally, changing the temperature necessarily alters the strength of the electrostatic interactions, making the decoupling even more

challenging [16]. Given the experimental challenges in decoupling chain length effects from overlapping state transitions and temperature-dependent electrostatic interactions in PILs, it is essential to leverage non-experimental techniques, such as advanced molecular dynamics simulations, to directly elucidate how chain length modulates their transport properties.

Molecular dynamics simulations have been extensively employed to investigate the fundamental properties of these materials using both atomistic and coarse-grained approaches [8]. While atomistic simulations with detailed force fields can elucidate critical dynamic and structural quantities [17, 18], they are computationally expensive. Computing properties such as diffusivity and chain relaxation times requires extensive simulations with large system sizes, particularly for longer polymer chains, thereby significantly increasing computational costs. To mitigate these limitations, coarse-graining techniques can be used [8, 19]. In this approach, groups of atoms and molecules are mapped onto coarse-grained beads, preserving essential features such as mass and charge distributions. By reducing the degrees of freedom of the system to the necessary complexity required to observe desired properties, coarse-graining allows for an efficient way to probe system features. The current standard for hard sphere, bead-spring polymer models relies primarily on Lennard-Jones forces and Coulomb interactions to model non-bonded interactions between beads on different chains [20]. Notably, the Kremer-Grest model [21, 22] has been used to probe important structural properties. However, due to the rigid excluded-volume interactions inherent in hard-sphere models, simulations often fall short in capturing the nuanced, large-scale behavior of systems featuring long poly anions, where particle deformation, interpenetration, and dense packing are critical phenomena [23]. In contrast, soft-sphere models offer a more realistic alternative by accommodating the flexibility of particle interactions, allowing for better modeling at larger length scales. Additionally, hard-sphere models struggle to model charge delocalization and encounter divergences in potential energy when particle spheres overlap - a problem that necessitates restricted time stepping and therefore additional computational limits [23].

Alternatively, methods like Dissipative Particle Dynamics (DPD) use soft spheres that can overlap, enabling the representation of larger numbers of molecules and facilitating the efficient probing of mesoscale properties and system sizes. DPD employs both dissipative and random forces alongside conservative interactions to capture hydrodynamic and thermal fluctuations. This simulation method allows

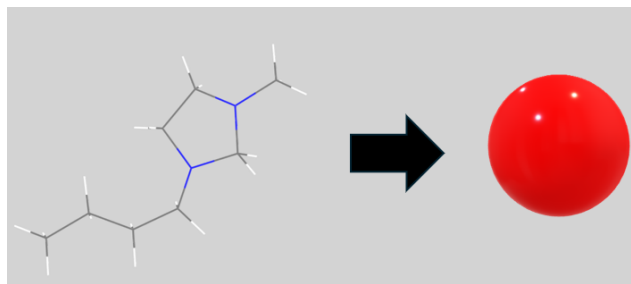


Figure 1.1: Example coarse graining of ionic liquid monomer [BMIM+] [24] into a hard sphere

DPD to replicate momentum transfer and energy dissipation at the mesoscopic scale, making it particularly useful for capturing dynamic properties such as diffusion and collective motion observed in PIL systems [25, 26]. DPD's soft-sphere interactions also allow it to more effectively model systems requiring flexibility and dense packing without the stringent limitations on time stepping [8]. However, when electrostatic potentials are incorporated, there is no closed-form analytical solution for the Ewald summation, necessitating computationally intensive calculations that can diminish the computational speed-up offered by modern GPU-accelerated computing [23].

The Gaussian core model developed by Ben Ye and the Wang group, as outlined in Appendix A of this work [23, 27], provides a computationally efficient method for modeling these systems using soft spheres. It enables the simulation of larger, fully entangled systems to obtain dynamic and experimentally relevant quantities, which we have set out to achieve in this thesis.

Experimental studies have observed that polymerized ionic liquids exhibit higher conductivity than their monomeric counterparts even at ambient temperature, though the underlying mechanism remains unresolved [28]. While, molecular dynamics simulations using Lennard-Jones hard sphere models similarly indicate a conductivity increase that persists up to a chain length of 25, these studies do not examine the relevant dynamic properties [29, 30]. Moreover, the behavior of these systems beyond the unentangled regime, into the partially entangled, and fully entangled regimes remains unclear. This paper primarily investigates whether isolating the effect of increasing PIL chain length leads to a continued enhancement in conductivity and evaluates the extent to which chain length can serve as an effective tuning parameter for these systems. To address these questions, we employ our Gaussian Core Model for its computational efficiency and its ability to replicate the essential

features of PIL systems, thereby allowing us to systematically isolate the influence of chain length on conductivity and constituent dynamic properties.

## References

1. Fong, K. D., Self, J., McCloskey, B. D. & Persson, K. A. Ion Correlations and Their Impact on Transport in Polymer-Based Electrolytes. *Macromolecules* **54**, 2575–2591 (2021).
2. Hickner, M. A. Ion-containing polymers: new energy & clean water. *Materials Today* **13**, 34–41 (2010).
3. Kusoglu, A. & Weber, A. Z. New insights into perfluorinated sulfonic-acid ionomers. *Chemical Reviews* **117**, 987–1104 (2017).
4. Strakosas, X., Bongo, M. & Owens, R. M. The organic electrochemical transistor for biological applications. *Journal of Applied Polymer Science* **132**, 41735 (2015).
5. Lebedeva, O., Kultin, D. & Kustov, L. Polymeric Ionic Liquids: Here, There and Everywhere. *European Polymer Journal* **203**. Review article, 112657 (2024).
6. Correia, D. M. *et al.* Ionic Liquid Polymer Composites: A New Platform for Multifunctional Applications. *Advanced Functional Materials* **30** (2020).
7. Zhang, S.-Y. *et al.* Poly(ionic liquid) composites. *Chem. Soc. Rev.* **49**, 1726–1755 (6 2020).
8. Shen, K.-H., Fan, M. & Hall, L. M. Molecular Dynamics Simulations of Ion-Containing Polymers Using Generic Coarse-Grained Models. *Macromolecules* **54**, 2031–2052 (2021).
9. Qian, W., Texter, J. & Yan, F. Frontiers in poly(ionic liquid)s: syntheses and applications. *Chemical Society Reviews* **46**, 1124–1159 (2017).
10. Matsumoto, K., Yano, T., Date, S., Odahara, Y. & Narimura, S. Synthesis of imidazolium-based poly(ionic liquid)s and their application to ion-exchange materials. *Polymer Bulletin* **78**, 5165–5180 (2021).
11. Imbrogno, J. *et al.* Relationship between Ionic Conductivity, Glass Transition Temperature, and Dielectric Constant in Poly(vinyl ether) Lithium Electrolytes. *ACS Macro Letters* **10**, 1002–1007 (2021).
12. Rubinstein, M. & Colby, R. H. *Polymer Physics* (Oxford University Press, Oxford ; New York, 2003).
13. Jeddi, J., Niskanen, J., Lessard, B. H. & Sangoro, J. Ion transport in polymerized ionic liquids: a comparison of polycation and polyanion systems. *Faraday Discussions* **253**. Received 29th March 2024, Accepted 15th May 2024, First published 17th May 2024, 426–440 (2024).

14. Reiter, M. *et al.* Tuning the glass transition of siloxane-based poly(ionic liquid)s towards high ion conductivity. *Journal of Polymer Science* **59**, 1518–1527 (2021).
15. Wojnarowska, Z. *et al.* Effect of Chain Rigidity on the Decoupling of Ion Motion from Segmental Relaxation in Polymerized Ionic Liquids: Ambient and Elevated Pressure Studies. *Macromolecules* (2017).
16. Bocharova, V. *et al.* Influence of Chain Rigidity and Dielectric Constant on the Glass Transition Temperature in Polymerized Ionic Liquids. *The Journal of Physical Chemistry B* **121**, 11511–11519 (2017).
17. Gartner, T. E. & Jayaraman, A. Macromolecules. *Macromolecules* **52**, 755–786 (2019).
18. Joshi, S. Y. & Deshmukh, S. A. Molecular Simulations. *Molecular Simulation* **47**, 786–803 (2021).
19. Wang, Y.-L., Li, B. & Laaksonen, A. Coarse-grained simulations of ionic liquid materials: from monomeric ionic liquids to ionic liquid crystals and polymeric ionic liquids. *Phys. Chem. Chem. Phys.* **23**, 19435–19456 (35 2021).
20. Weeks, J. D., Chandler, D. & Andersen, H. C. Role of repulsive forces in determining the equilibrium structure of simple liquids. *Journal of Chemical Physics* **54**, 5237–5247 (1971).
21. Kremer, K. & Grest, G. S. Dynamics of entangled linear polymer melts: A molecular-dynamics simulation. *The Journal of Chemical Physics* **92**, 5057–5086 (1990).
22. Ganesan, V. Ion transport in polymeric ionic liquids: recent developments and open questions. *Molecular Systems Design & Engineering* **4**, 280–293 (2019).
23. Ye, B. B., Chen, S. & Wang, Z.-G. GCMe: Efficient Implementation of the Gaussian Core Model with Smeared Electrostatic Interactions for Molecular Dynamics Simulations of Soft Matter Systems. *Journal of Chemical Theory and Computation* **20**, 6870–6880 (2024).
24. Schrödinger, LLC. *Schrödinger Release 2025-1: Maestro* Schrödinger, LLC (New York, NY, 2025).
25. Curk, T. Dissipative particle dynamics for coarse-grained models. *Journal of Chemical Physics* **160**, 174115 (2024).
26. Español, P. & Warren, P. B. Perspective: Dissipative particle dynamics. *Journal of Chemical Physics* **146**, 150901 (2017).
27. Ye, B., Walker, P. & Wang, Z.-G. MDCraft: A Python assistant for performing and analyzing molecular dynamics simulations of soft matter systems. *Journal of Open Source Software* **9**, 7013 (Aug. 2024).
28. Griffin, P. J. *et al.* Ion Transport in Cyclopropenium-Based Polymerized Ionic Liquids. *Macromolecules* **51**, 1681–1687 (2018).

29. Fong, K. D., Self, J., McCloskey, B. D. & Persson, K. A. Onsager Transport Coefficients and Transference Numbers in Polyelectrolyte Solutions and Polymerized Ionic Liquids. *Macromolecules* **53**, 9158–9167 (Oct. 2020).
30. Zhang, Z., Wheatle, B. K., Krajniak, J., Keith, J. R. & Ganesan, V. Ion Mobilities, Transference Numbers, and Inverse Haven Ratios of Polymeric Ionic Liquids. *ACS Macro Letters* **9**, 84–89 (2020).

*Chapter 2***DYNAMICS OF GAUSSIAN CORE MODELED POLYIONIC LIQUID SYSTEMS**

In this chapter, we examine the dynamic properties of a polymerized ionic liquid system using the Gaussian core model described in Appendix A. We derive and analyze the fundamental characteristics of the system—including the radius of gyration, diffusivity, relaxation time, and ion conductivity—and investigate how these properties scale with polymer chain length,  $N$ . Furthermore, we employ the Onsager transport framework to compute and tabulate the relevant transport coefficients, thereby linking molecular trajectories to bulk transport properties. The system is modeled as a coarse-grained polyanion, where each bead carries a single negative charge and is paired with a cation carrying a single positive charge. Each simulation contains equal quantities of anionic and cationic monomer beads, with no solvent present - modeling a polymerized ionic liquid in the ionic density limit. In summary, this modeling approach bridges microscopic dynamics with macroscopic transport behavior, allowing for insight into the properties and ultimately design of advanced polymerized ionic liquids for material applications.

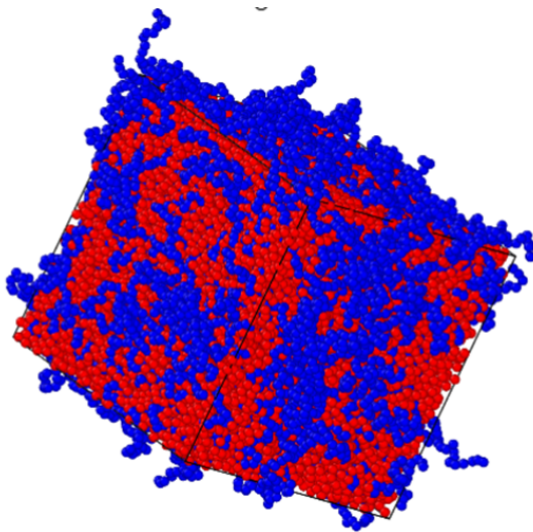


Figure 2.1: Example system snapshot for a polyanion (blue) and cation (red) system with chain length,  $N = 50$  - visualized using Ovito [1]

## 2.1 Methodology

The molecular dynamics simulations for this section were performed using OpenMM [2] in the NVT, canonical ensemble. The system has at least 48,000 identically sized, coarse grained, charged monomer particles ( $N_p$ ) - with longer chain systems having up to 118,000 particles and there is no solvent in the system. Chain length  $N$ , of the polyanion was varied from 1 to 350, while the cation remained monomeric for all simulations. A standard temperature of  $T = 300$  K was maintained a DPD thermostat [3] for the Onsager coefficients and ionic conductivity calculations - this thermostat was selected in order to capture the hydrodynamic and diffusive effects at both short and long chain lengths. Again, the system is modeled as solvent free, with an equal number of symmetric polyanion and cation beads in the melt. These simulations rely on the Gaussian Core Model, outlined in Appendix A, of this paper with smeared electrostatics and mass to coarse grain the monomer beads. Bonds between connecting polyanion chains were modeled by a harmonic bond potential [4]. As a point of comparison, a uncharged system with identical system set up and parameterization to the charged system where only the system charges are removed.

$$u_{harm}(r_{ij}) = \frac{1}{2}k(r_{ij} - b)^2 \quad (2.1)$$

where the force constant  $k_{ij}$  is  $100 k_b T / d^2$ , and the equilibrium bond length  $b = .8d$ , and  $d$  is the characteristic length scale, defined formally in A.10. The polarization of the fluid is accounted for by the relative permittivity ( $\epsilon_r = 12$ ), which is within the standard range of values for ionic liquids [5, 6].

The systems are initialized by determining the appropriate box dimensions ( $L_x, L_y, L_z$ ) and volume to accommodate the system, constrained by the system density and total number of particles ( $N_p$ ):

$$L_z = \left( \frac{N_p}{\rho} \right)^{\frac{1}{3}} \quad (2.2)$$

All system dimensions are equal, and periodic boundary conditions are applied in all directions. For example, the system size for a 48,000-particle system is  $288 \text{ \AA} \times 288 \text{ \AA} \times 288 \text{ \AA}$ . The system is then randomly populated with polyanions ( $N_p/(2N)$ ) and cations ( $N/2$ ).

A local energy minimization is performed before the system is simulated over a time scale sufficient to capture its dynamics. The time step size is  $t = 0.02\tau$ , where  $\tau$  is

the characteristic time scale as defined in A.11. Because, as we show later in this paper, the relaxation time of the system scales as  $\sim N^{3.0}$  (figure 2.4), the runtime can vary significantly depending on the chain length.

For the special case, where we are applying an electric field to the system, the field strength is calculated based on the potential difference (in units  $k_b T/e$ ), scaled by the system dimensions, ensuring consistency with physical units. This electric field is then introduced along the specified axis (the z axis in this case) while accounting for the system's dielectric properties.

## 2.2 Results and Discussion

### Radius of Gyration

The radius of gyration,  $R_g$  can be a useful quantity to understand the dimensions of a polymer and give insight into scaling relationships with other properties like diffusivity. It is defined as the root mean square of the distances between the center of mass of the polymer,  $\mathbf{R}_c$  and the position vectors of each constituent monomer,  $\mathbf{r}_i$  (both vector quantities, represented by bolded text). [7].

$$R_g = \sqrt{\frac{\sum_{i=1}^N m_i \|\mathbf{r}_i - \mathbf{R}_c\|^2}{\sum_{i=1}^N m_i}} \quad (2.3)$$

For an ideal chain obeying random walk scaling, the radius of gyration scales with  $N^{\frac{1}{2}}$  [7, 9]. Similarly, for standard (non-ionic) polymers in a melt, where excluded volume interactions are screened out by densely packed monomers, we also expect the radius of gyration to scale with an exponent of  $\frac{1}{2}$  [7]. That is to say  $R_g \propto N^\xi$ , where  $\xi = \frac{1}{2}$ . Indeed, we get back almost precisely this relationship at large chain lengths ( $N > 200$ ) for our charged polyanion system 2.2.

It can be helpful to compare our system to an identical polymer melt where the polymer and its counter-ions have identical parameterization but without any charge. While in figure 2.2 we get back an identical scaling relationship with N of  $R_g \propto N^{.5}$  for both systems, the consistent difference in size for the charged system compared with the uncharged system highlights the residual electrostatic repulsion even in the highly screened ionic liquid density limit.

### Relaxation Time

The orientational relaxation time of a polymer, denoted as  $\tau_r$ , is an important parameter for determining the duration over which a polymer loses correlation with

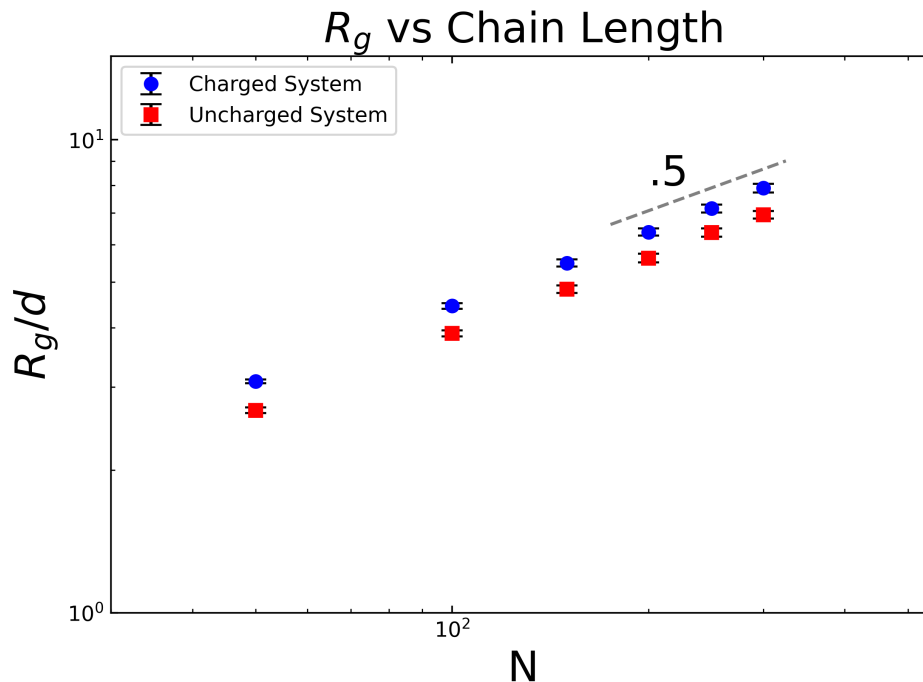


Figure 2.2: Radius of gyration for polyanion and neutral system polymers as a function of the chain length, showing a scaling relationship of .52 for the charged system and .53 for the uncharged system [8]

its initial orientation. This relaxation time can be efficiently calculated from the end-to-end autocorrelation function,  $C_{ee}(t)$  [7] as shown below, where  $R_{ee}$  is the end to end distance of a polymer:

$$\begin{aligned} \mathbf{R}_{ee}(t) &= \mathbf{r}_N - \mathbf{r}_1, \\ C_{ee}(t) &= \frac{\langle \mathbf{R}_{ee}(t) \cdot \mathbf{R}_{ee}(0) \rangle}{\langle \mathbf{R}_{ee}^2 \rangle}. \end{aligned} \quad (2.4)$$

The autocorrelation function  $C_{ee}(t)$ , expressed as a function of the dot product, converges to zero at sufficiently large times. This relaxation behavior can be modeled by fitting  $C_{ee}(t)$  to a stretched exponential function. The relaxation time of the polyanions is then determined by integrating the stretched exponential function, which involves the gamma function [10], as shown below:

$$C_{ee}^{fit}(t) = \exp \left[ - \left( \frac{t}{\tau_{fit}} \right)^\beta \right] \quad (2.5)$$

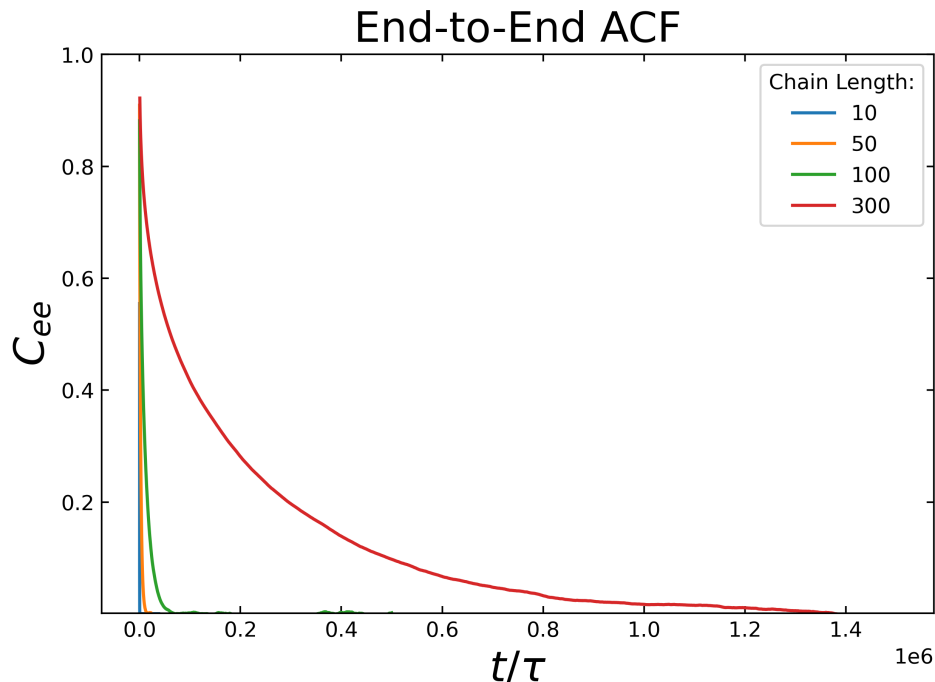


Figure 2.3: End to end autocorrelation function plotted against time for a range of chain lengths

$$\tau_r = \int_0^{\infty} C_{ee}^{fit}(t) dt = \frac{\tau_{fit}}{\beta} \Gamma\left(\frac{1}{\beta}\right) \quad (2.6)$$

where  $\tau_r$  is the relaxation time, and  $\tau_{fit}$  and  $\beta$  are fitting parameters. Finally, the gamma function defined as:

$$\Gamma(\beta) = \int_0^{\infty} e^{-t} t^{\beta-1} dt \quad (2.7)$$

For a fully entangled uncharged polymer, the relaxation time typically scales with the cube of chain length, that is to say,  $\tau_r \propto N^3$ . For polymers in the transition regime, where they are only partially entangled,  $\tau_r \propto N^\xi$  for  $2 < \xi < 3$ .

Looking at our system in both the transition region ( $N < 150$ ) and what would typically be considered the entangled region ( $N > 150$ ), we observe the expected behavior for an ideal chain in both regime. This apparent adherence to standard reptation scaling of  $\tau_r \propto N^3$  would imply that the charged polymers are fully entangled with one another and behave relatively ideal in the solvent-free polyionic liquid limit. This adherence is significant, as we can expect or chains to continue to exhibit ideality in dynamic scaling properties like diffusivity.

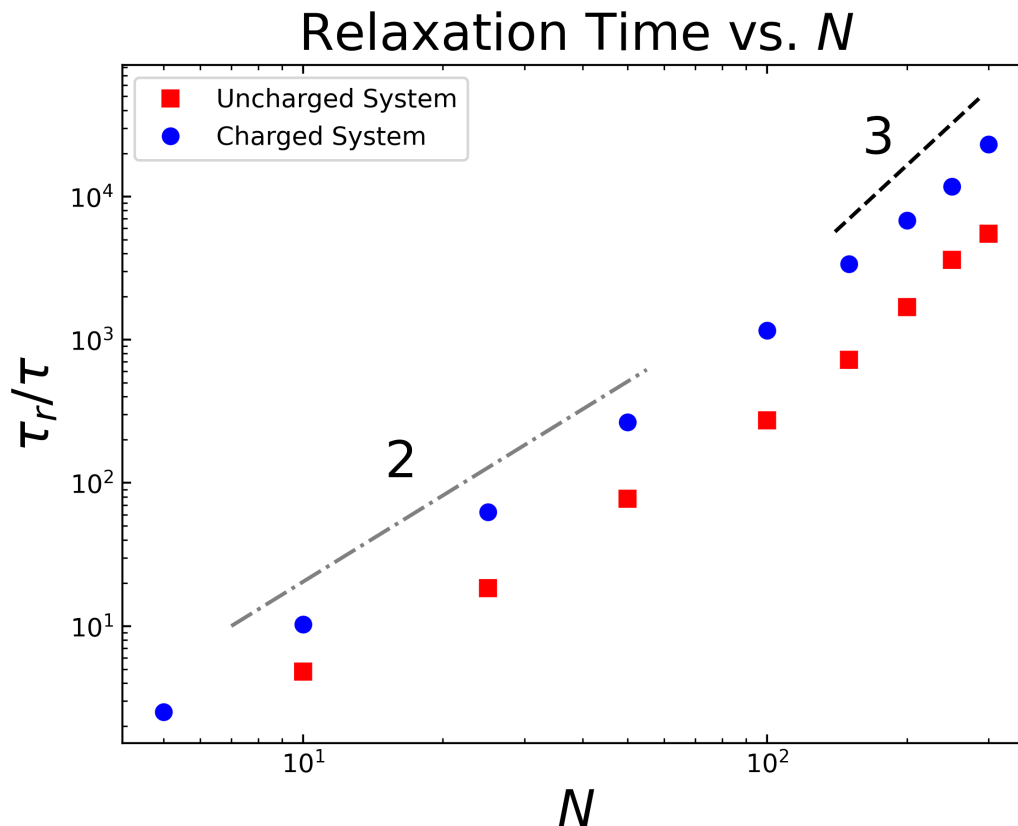


Figure 2.4: Plot of relaxation time vs. chain length for polyanions in our polymerized ionic liquid system compared to an identical uncharged system, showing scaling relationship of  $\sim N^{3.00}$  in the fully entangled region. Note the scaling in the transition regime is  $\sim N^{2.25}$  ( $25 < N < 100$ ) and  $\tau$  here is the characteristic time scale defined in equation A.11

By way of comparison it is helpful to compare this behavior to that of our identical uncharged system portrayed by the blue data points in figure 2.4. Similar to the charged system, in our uncharged system, we can see the same expected adherence to reptation scaling of  $\tau_r \propto N^3$ . However, it is important to recognize that our charged system relaxes substantially slower than the uncharged counterpart in both the transition and fully-entangled regimes. The charged polymers relax more slowly because the electrostatic interactions between them and their counter-ions, that increase friction and create additional dynamic constraints, hindering chain motion. This extra resistance delays relaxation in both the transition and fully entangled regimes, even though both systems follow the same scaling.

## Diffusion

Diffusion behavior as a function of chain length is not only an experimentally relevant transport property but also a key factor in uncovering fundamental transport mechanisms and providing valuable insights into material behavior. We compute the per-particle diffusivity directly from the per-particle averaged mean squared displacement [11, 12]:

$$\text{MSD} = \left\langle \frac{1}{N_p} \sum_{i=1}^{N_p} (\mathbf{r}_i(0) - \mathbf{r}_i(t))^2 \right\rangle \quad (2.8)$$

where  $i$  is the particle index, and  $N_p$  remains our number of total particles for a species. Ultimately deriving our diffusion coefficient from our mean squared displacement - note 6 as coefficient comes from our three dimensional system [7].

$$D = \frac{\text{MSD}}{6t} = \frac{1}{6} \lim_{t \rightarrow \infty} \frac{d}{dt} \left\langle \frac{1}{N_p} \sum_{i=1}^{N_p} (\mathbf{r}_i(0) - \mathbf{r}_i(t))^2 \right\rangle \quad (2.9)$$

We can further explicitly write this expression in terms of chain center of mass,  $\mathbf{R}_c$ , to get our polymer diffusivity  $D_-$ . Where we instead sum over our total number of polymers,  $n$ , noting that  $n = \frac{N_p}{N}$  and in our constant density system is a function solely of chain length:

$$D_- = \frac{1}{6} \lim_{t \rightarrow \infty} \frac{d}{dt} \left\langle \frac{1}{n} \sum_a^n [\mathbf{R}_c^a(t) - \mathbf{R}_c^a(0)]^2 \right\rangle \quad (2.10)$$

here,  $a$  is the chain index. We can determine the diffusion coefficient from the mean squared displacement using either the position vectors of the individual constituent monomers or the position vectors of the polymer's center of mass. For this analysis we calculated diffusion coefficients for the central fifth of monomer beads as well as the center of mass to ensure consistency between the two forms. However, the central bead displacement is used throughout the analysis in section 2.4. Figure 2.5 portrays the central bead diffusivity showing the scaling relationship between chain length and polymer diffusivity.

For an uncharged polymer in the fully entangled regime, we expect the diffusivity to scale with  $N^{-2}$ . In our charged system, we can conduct a dimensional analysis of our scaling laws [13] and determine that we should expect our diffusion to scale with  $N^{-1.96}$ , considering both our relaxation time and our radius of gyration - similarly we would expect our uncharged system to scale with  $N^{-1.92}$ . This approach provides a way to corroborate our diffusivity scaling results for our polyanion:

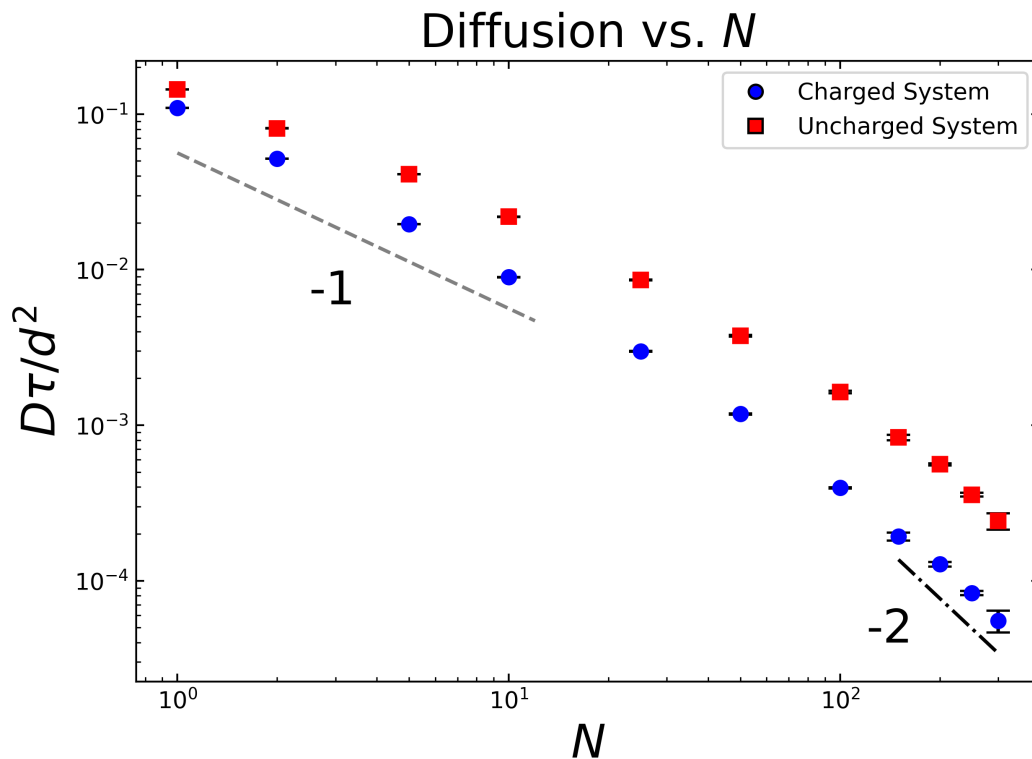


Figure 2.5: Diffusivity vs. chain length showing an unentangled scaling relationship of  $N^{-1.08}$  system and a reptation scaling relationship of approximately  $N^{-2.06}$  for our polyanion. Similarly, the uncharged system shows a scaling relationship of  $N^{-.97}$  and  $N^{-2.06}$  in the unentangled and entangled regimes respectively.

$$D[=] \frac{R_g^2}{\tau_r} \approx \frac{N^{1.04}}{N^{3.00}} \approx N^{-1.96} \quad (2.11)$$

Our dimensional analysis confirms our molecular dynamics analysis for our scaling law where our diffusivity scales at the expected  $N^{-2}$  from typical reptation regime. From this we can conclude that our chains follow ideal scaling behavior, with our polyanion chains moving slower as a result of the electrostatics.

For internal consistency, figure 2.6 shows the center of mass diffusivity, compared to the central bead diffusivity for our charged system. The key takeaway here is that our central bead displacement correctly models the center of mass for each polymer - at sufficiently long time.

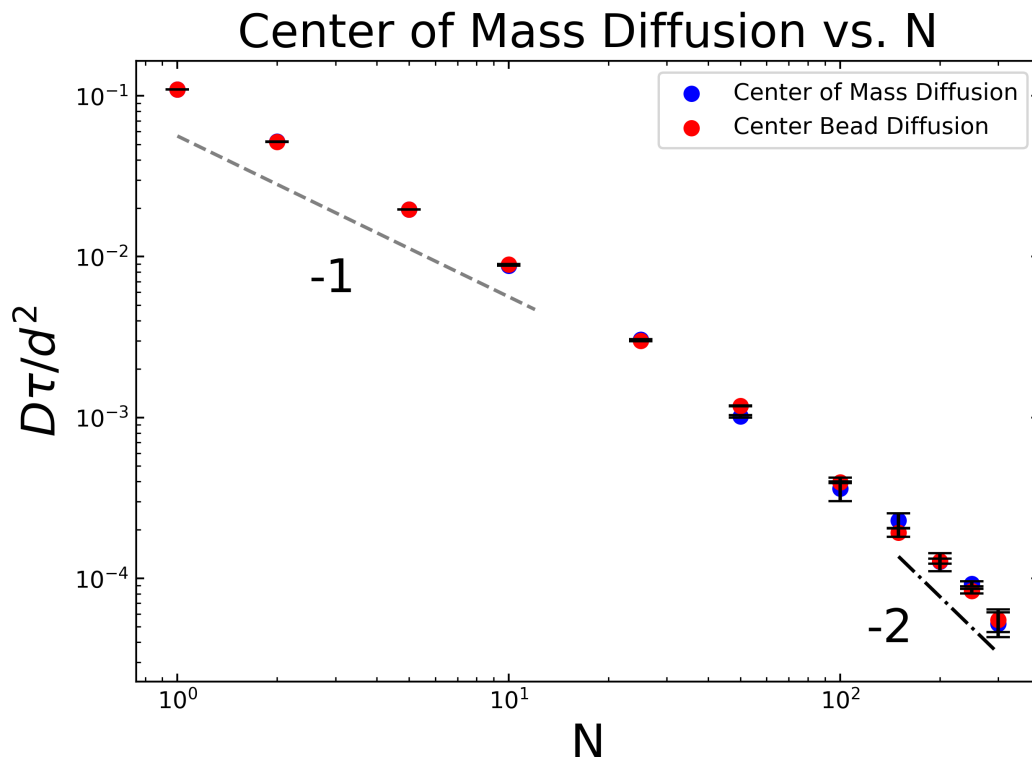


Figure 2.6: Center of mass diffusivity for the charged polyanion system compared to central bead diffusion, showing agreement between the two methods, even at our longer chain lengths

### Onsager Transport Coefficients

The Onsager transport framework, [11] represents an intuitive way in molecular dynamics of characterizing electrolyte transport phenomena from the system flux. It is particularly useful in systems where the traditional Nernst-Einstein ideal solution transport relationship, driven mostly by system diffusion, breaks down. Here the flux of species  $i$ ,  $J_i$  can be characterized by the sum of the Onsager transport coefficients and their corresponding chemical potentials:

$$J_i = - \sum_j L_{ij} \nabla \bar{\mu}_j \quad (2.12)$$

where  $\bar{\mu}_j$  is the electrochemical potential of each species indexed at  $j$ . From there we can calculate the Onsager transport coefficients from the particle positions using a similar Einstein relation scheme as diffusivity in equation 2.11, where the Onsager transport coefficient between species  $i$  and  $j$ ,  $L_{ij}$  is:

$$L_{ij} = \frac{1}{6k_bTV} \lim_{t \rightarrow \infty} \frac{d}{dt} \left\langle \sum_{\alpha} [\mathbf{r}_{i,\alpha}(t) - \mathbf{r}_{i,\alpha}(0)] \cdot \sum_{\beta} [\mathbf{r}_{j,\beta}(t) - \mathbf{r}_{j,\beta}(0)] \right\rangle \quad (2.13)$$

where  $i$  and  $j$  in our case each represent a positive or negative ion,  $\beta$  and  $\alpha$  represent each particle and the denominator,  $k_bTV$ , represent the Boltzman constant, the temperature, and fixed volume of our system respectively. Because of the symmetric nature of the function,  $L_{+-} = L_{-+}$ , ie, the cation/anion correlation term is identical to its corresponding cross term. If we evaluate each particle,  $\mathbf{r}_{i,\alpha}(t)$  relative to the system center of mass at time  $t$ , we can further conclude that the individual mass flux for each species must sum to zero,  $\sum_i M_i J_i = 0$  [14]. This relationship constrains our Onsager Coefficients for each species as,  $\sum_i M_i L_{ij}$ . Four our two species system composed entirely of anion/cation particles with the same mass, it then follows that  $M_+(L_{++} + L_{+-}) = M_-(L_{--} + L_{-+}) = 0$  and thus  $L_{--} = L_{++} = -L_{+-}$ . As a result the values of the respective Onsager transport coefficients,  $L_{ij}$ , are intrinsically linked, where an increase in one must cause a decrease in another. Larger values of those coefficients demonstrates an increase in correlated motion, while decreasing values of a coefficient imply an increase in anticorrelated motion, this is illustrated in figure 2.8. In the case of the same species Onsager coefficient  $L_{ii}$  the equation simplifies to:

$$L_{ii} = \frac{1}{6k_bTV} \lim_{t \rightarrow \infty} \frac{d}{dt} \left\langle \sum_{\alpha} \sum_{\beta} [\mathbf{r}_{i,\alpha}(t) - \mathbf{r}_{i,\alpha}(0)] \cdot [\mathbf{r}_{i,\beta}(t) - \mathbf{r}_{i,\beta}(0)] \right\rangle \quad (2.14)$$

In the case of our polymer it can be more natural to further simplify this term into a summation over each chain and its constituent particles:

$$L_{--} = \frac{1}{6k_bTV} \lim_{t \rightarrow \infty} \frac{d}{dt} \left\langle \sum_a \sum_{\alpha} [\mathbf{r}_{a,\alpha}(t) - \mathbf{r}_{a,\alpha}(0)] \cdot \sum_b \sum_{\beta} [\mathbf{r}_{b,\beta}(t) - \mathbf{r}_{b,\beta}(0)] \right\rangle \quad (2.15)$$

where  $a$  and  $b$  are now the chain indices, and  $\alpha$  and  $\beta$  are particle index on each chain. We can further transform this relation in terms of chain center of mass,  $\mathbf{R}_c$  - a more natural representation that allows for direct continuation with our previous scaling arguments.

$$L_{--} = \frac{N^2}{6k_bTV} \lim_{t \rightarrow \infty} \frac{d}{dt} \left\langle \sum_a [\mathbf{R}_c^a(t) - \mathbf{R}_c^a(0)] \cdot \sum_b [\mathbf{R}_c^b(t) - \mathbf{R}_c^b(0)] \right\rangle \quad (2.16)$$

noting again that the chain center of mass  $\mathbf{R}_c = \frac{1}{N} \sum_{\alpha} \mathbf{r}_{a,\alpha}$ , which leads to the multiplicative inclusion of the  $N^2$  term into the prefactor. If we exclude the instance where  $\beta = \alpha$  from the summation, we get our  $L_{--}^{distinct}$  term. Finally, in the special case of when  $\beta = \alpha$ , for our "self" term,  $L_{ii}^{self}$ , we can derive the following:

$$L_{ii}^{self} = \frac{1}{6k_bTV} \lim_{t \rightarrow \infty} \frac{d}{dt} \left\langle \sum_{\alpha} [\mathbf{r}_{i,\alpha}(t) - \mathbf{r}_{i,\alpha}(0)]^2 \right\rangle \quad (2.17)$$

Making the same transformation we did in equations 2.15, 2.16 we can arrive at a center of mass expression of our polyanion term for the self contribution:

$$L_{--}^{self} = \frac{N^2}{6k_bTV} \lim_{t \rightarrow \infty} \frac{d}{dt} \left\langle \sum_a [\mathbf{R}_c^a(t) - \mathbf{R}_c^a(0)]^2 \right\rangle \quad (2.18)$$

Formally it follows that:

$$L_{ii} = L_{ii}^{distinct} + L_{ii}^{self} \quad (2.19)$$

Where the  $L_{--}^{distinct}$  term accounts for only interchain interactions and the  $L_{++}^{distinct}$  term accounts for all cation interactions not captured by the mean squared displacement. Finally, comparing equation 2.11 with 2.17 and 2.10 with 2.18 we can see the direct relationship between the self term and diffusivity below:

$$L_{ii}^{self} = \frac{D_i n_i N_i^2}{k_bTV}, \quad L_{++}^{self} = \frac{D_+ n_+}{k_bTV}, \quad L_{--}^{self} = \frac{D_- n_- N^2}{k_bTV} \quad (2.20)$$

where  $n_i$  is the total molecules of species  $i$  in the system, while  $N$  is still the chain length. By inspection, we can see that  $L_{++}^{self}$  is directly proportional to the cation diffusivity. It is important to remember here that the monomeric species concentration remains fixed and equal (eg.  $\frac{n_i N_i}{V}$ ) regardless of species or chain size. We therefore can conclude that  $L_{--}^{self}$  must have  $N^1$  proportionality to the diffusivity of that species. Additionally, the self terms are necessarily positive contributions to their respective coefficients, given the intrinsically positive nature of the mean squared displacement. For ion carriers with application to energy storage, it is desirable to have uncorrelated anion to cation motion, and correlated anion to anion, cation to cation motion. Under an applied potential, the decoupled ion motion lowers the frictional drag on charge carriers, which means that during charging or discharging the ions move more freely and energy losses are minimized.

For our system, illustrated in figure 2.7, we see a steady magnitude of correlated motion for our polyanion when we increase chain length, which comports with results found in similar studies of solvent free but shorter chained polymer electrolytes systems [15].

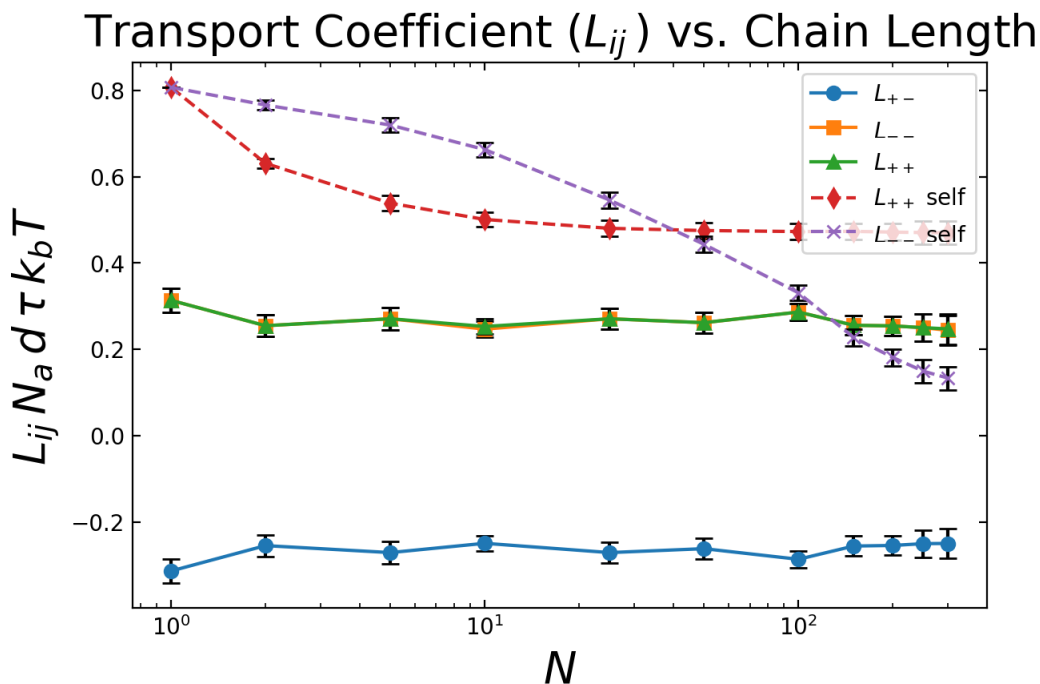


Figure 2.7: Onsager transport coefficients for polyanion system. Note the  $L_{++}$  and  $L_{--}$  overlap near-perfectly and may not be distinguishable

Dynamics of electrolyte solutions in the ionic liquid limit are governed by electrostatic interactions, short screening lengths due to dense packing, and diffusive driven motion [16, 17]. These conditions yield systems in which diffusion-induced perturbations are moderated by the opposing influences of electroneutrality and electrostatic repulsion. When looking at solvent-free PILs, we must also consider how the correlated movement of monomers along the same chain further complicates the dynamics.

Beginning our analysis with the  $L_{--}^{self}$  term (purple line) we observe a gradually increasing decline, indicating an increasing  $N$  dependence as chains become entangled. Accounting for the  $N$  dependence in equation 2.20 and the short chain diffusivity scaling relationship of  $\sim N^{-1}$ , it becomes clear that we should expect almost no change to  $L_{--}^{self}$  in the short chain regime ( $N < 10$ ) - this is borne out in the data where in the short chain regime we see a scaling relationship of  $\sim N^{-0.8}$ . As the

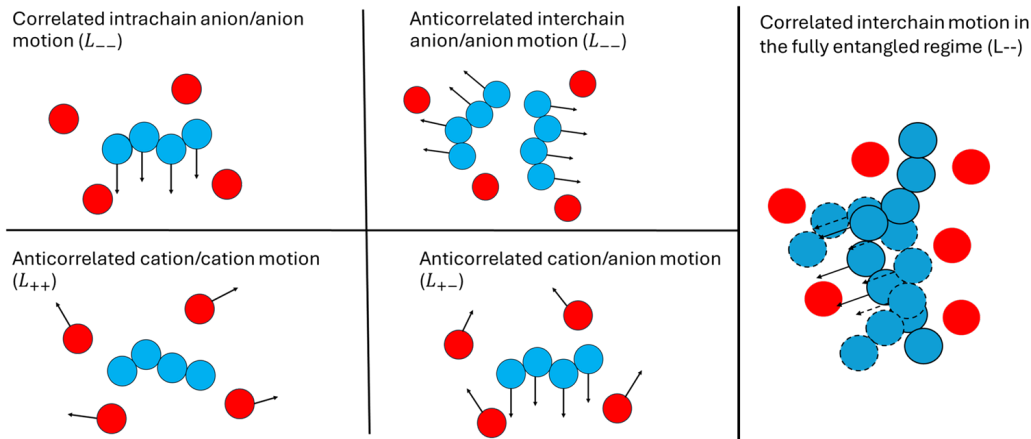


Figure 2.8: Illustration of correlated and anticorrelated anion/cation motion for our PIL system. 2.19

chains enter the semi-entangled and fully entangled regime, where the diffusivity scales with  $\sim N^{-2}$  we should expect  $L_{--}^{self}$  to begin to scale with  $\sim N^{-1}$ , and indeed the relationship in the fully entangled regime is  $\sim N^{-1.05}$ . The sudden and then more subtle decrease in the  $L_{++}^{self}$  (red line), term corresponds to the transport limitations on the monomer as it's diffusion is hindered by an increasingly bulk polyanion. For our non-self terms, we can see a marked decline in correlated motion in the cross term,  $L_{+-}$ , coupled with a corresponding increase in the two remaining terms,  $L_{++}$  and  $L_{--}$ . Evaluating just our polyanion term,  $L_{--}$  (green/orange line), in the very short chain regime ( $N < 25$ ), the self component ( $L_{--}^{self}$ ) has a substantial, positive contribution to the overall term. This necessarily implies that the distinct contribution is negative, where electrostatics drive anticorrelated interchain interactions, as seen in figure 2.8. As chain length increases, correlated intrachain motion overtakes the decreasing contribution from the diffusive  $L_{--}^{self}$ , and the anticorrelated interchain contributions. The ultimate effect of this competition between these interactions is an increase in  $L_{--}$ , or anion correlated motion as chain length enters the Rouse regime - ultimately tapering off and decreasing slightly once fully entangled. Again, making a direct comparison with our uncharged system can be helpful for this analysis, as shown in figure 2.9, where the system's Onsager coefficients follow the same general trend. However, the marked increase in the magnitude of the uncharged polymer correlation (red line) relative to the polyanion (blue line) indicates that electrostatics dampen polymer correlated motion. It follows that this loss of correlation results from electrostatic repulsion between like species.

Noting again that in our binary, uniform mass polyanion system we can show that

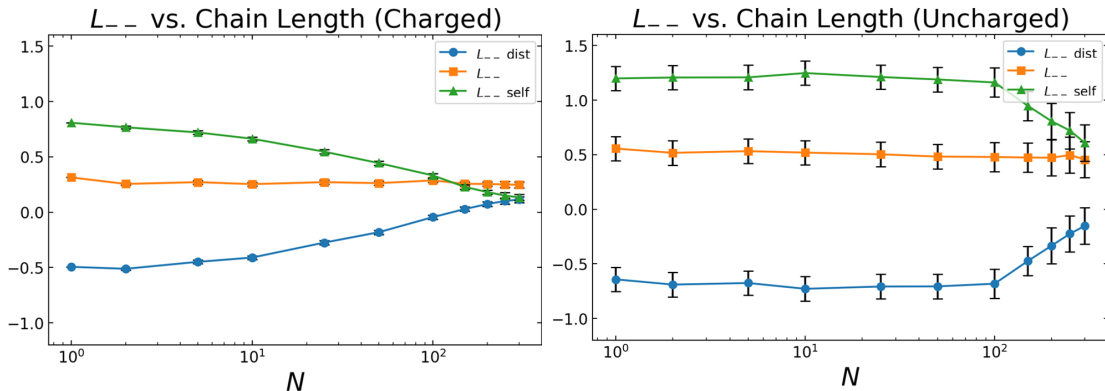


Figure 2.9:  $L_{--}$  for both charged and uncharged system plotted against chain length for direct comparison. Note for both two component systems where all particles have the same mass,  $L_{--}$  contains the same information as the other two Onsager Coefficients.

$L_{--} = L_{++} = -L_{+-}$ , it is expected that our cation and cross terms are equal and opposite respectively of our polyanion term. Physically, the cations begin and remain anticorrelated with one another driven by repulsive electrostatic interactions and incompressibility - the relationship in equation 2.19 and a dominant self term (red line in figure 2.7) implies a negative contribution from the 'distinct' cation interactions. An initial increase in  $L_{++}$  in the short chain region represents increasingly correlated motion between cations, driven by system incompressibility response to increasingly correlated polyanions. Intuitively the same analysis is used to justify anti-correlated motion between cations and anions - resulting in a negative  $L_{+-}$  term. From figure 2.9 we can again note that the magnitude of our Onsager coefficient for our uncharged system is greater than that of our charged system. Considering the cross species term,  $L_{+-}$ , this means that incompressibility drives this anticorrelated motion while short range electrostatic attraction between species dampens that affect.

### Ion Conductivity

Ion conductivity is a measure of the electrical conduction resulting from the motion of charged ions [18]. In our system, it quantifies the mobility of the two ion species, capturing both their diffusive and compensatory behavior. Maximizing this conductivity is important for designing and optimizing next-generation energy conversion and storage devices. Ion conductivity,  $\kappa$ , can be expressed in terms of the Onsager transport coefficients as seen below [19]:

$$\kappa = F^2 \sum_i \sum_j L_{ij} z_i z_j \quad (2.21)$$

where  $F$  is the Faraday constant, and  $z_i$  is the valency of the ion, which is  $\pm 1$  in our case. For our system, we can simplify this expression to be:

$$\kappa = F^2 (L_{++} + L_{--} - 2L_{+-}) \quad (2.22)$$

Since we have a binary mixture, where again  $L_{++} = L_{--} = -L_{+-}$  it follows that our conductivity can be expressed ultimately in terms of any single Onsager Coefficient, and we should expect it to follow similar trends. With that simplification in mind, our ion conductivity below, follows the same trend as our Onsager transport coefficients: [19].

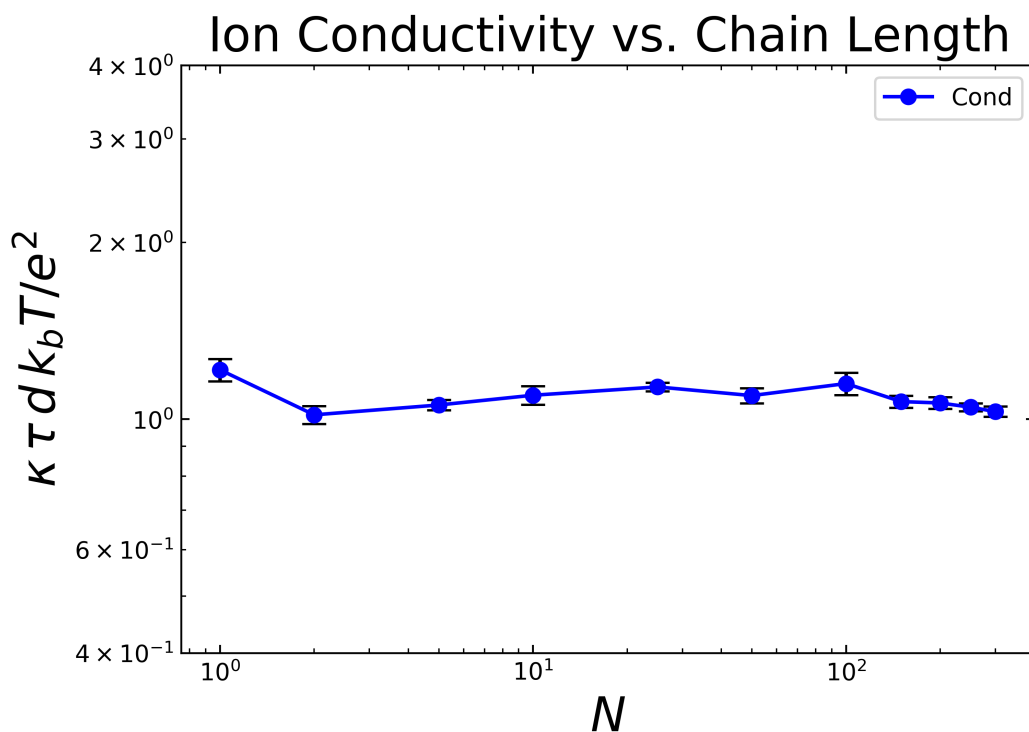


Figure 2.10: Ion conductivity calculated from Onsager transport coefficients for polyanion system

Excluding the monomer instance, the behavior in the short-chain regime aligns closely with previous molecular dynamics studies on shorter chain polyanions [11]. Where an increase in polyanion chain length leads to enhanced correlated motion, which directly contributes to a steady increase in ion conductivity. Moreover, as the polyanion enters the transition regime, we observe a steady albeit small uptick

in ion conductivity — an outcome consistent with the predicted behavior. In the fully entangled regime, we see a slight decline in conductivity, mirroring the drop in correlated motion in our Onsager Coefficients. These results underscore the limitations of chain length as a tuning parameter for polymerized ionic liquids in deployment as efficient charge transport materials.

These results are non-obvious when considering the traditional Nernst-Einstein method of calculating conductivity of an ideal solution [11], we can make a few manipulations to get a functional form with a more obvious scaling relationship with  $N$ :

$$\kappa^{NE} = \frac{e}{k_b T} (\rho_+ (z_+ e)^2 D_+ + \rho_- (z_- e)^2 D_-) = \frac{e^2}{V k_b T} (n_+ D_+ + n_- D_- N^2) \quad (2.23)$$

where,  $\rho_i$  is the number density,  $n_i$  is the molecules per species, and  $z_i$  is the species valence - remembering that our  $L_{--}^{self}$  which accounts for the whole chain, the valency is  $N$ . Accordingly, Nernst Einstein conductivity for an ideal electrolyte solution in the dilute limit should scale with the diffusivity of that system. Simplifying in terms of the Onsager transport coefficients - for consistency we can get:

$$\kappa^{NE} = F^2 (L_{++}^{self} + L_{--}^{self}) \quad (2.24)$$

Looking at figure 2.7 and equation 2.24, we would expect our conductivity to decrease as the diffusivity (or  $L_{ii}^{self}$  terms) decrease. This trend at first driven by the cation diffusivity,  $D_+$ , and then by the  $N$  dependent polyanion diffusivity,  $D_-$ , in the semi and entangled regimes. Comparing the two results, we can see that while the Nernst-Einstein conductivity decreases with chain length, our true conductivity remains relatively stable across chain length - seen in figure 2.11. Again, this effect is driven by the increase in correlated motion from the intrachain interactions. This effect can be seen to some degree experimentally [20], but these results might not be able to fully isolate the effects of increasing chain length versus the increasingly glassy behavior.

### Electric Field Calculated Ion Conductivity

Another method to measure ion conductivity is to apply an external, static electric field to our system, and calculate a conductivity directly from the system displacement response to the applied field [21]. To do this, we need to find the drift velocity,  $v_z$  by comparing the additional displacement from an applied electric field relative to that of a static, equilibrated system. We can also directly calculate the drift

## Ion Conductivity vs. NE Ion Conductivity

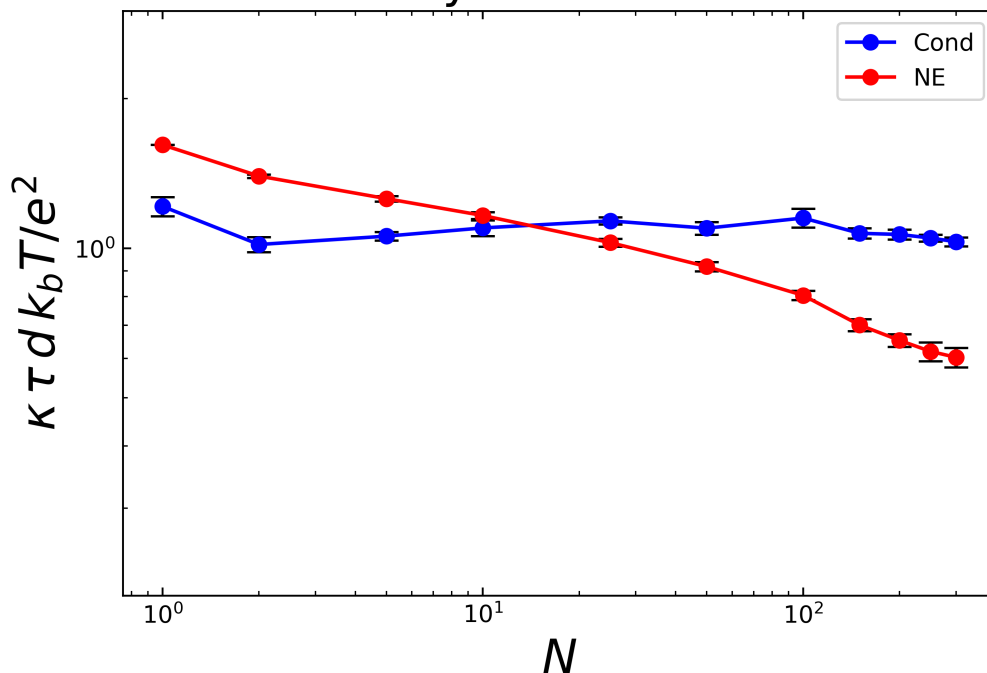


Figure 2.11: Conductivity and Nernst-Einstein Conductivity vs. Chain Length

velocity from the displacement in the direction of the electric field relative to the displacement orthagonal to that field. Below is the equation for finding the drift velocity for an electric field applied in the z direction.

$$\begin{aligned} \langle v_z \rangle^2 t^2 &= \langle (\mathbf{r}_z(t) - \mathbf{r}_z(0))^2 \rangle_E - \langle (\mathbf{r}_z(t) - \mathbf{r}_z(0))^2 \rangle_0 \\ &= \langle (\mathbf{r}_{\parallel}(t) - \mathbf{r}_{\parallel}(0))^2 \rangle_E - \langle (\mathbf{r}_{\perp}(t) - \mathbf{r}_{\perp}(0))^2 \rangle_E \end{aligned} \quad (2.25)$$

We can extract the average drift velocity directly from the mean squared displacement of our ions under the electric field by fitting  $a + bt^2$  to log-log, where a and b are fitting parameters, and  $\langle v_z \rangle = \sqrt{b}$ . This is done at sufficiently long time where the slopes of the log-log mean squared displacement in the parallel direction are 2 and the orthagonal directions are 1. An example of this can be seen in figure 2.12

Using the average drift velocity, we can directly calculate the average electrophoretic mobility and ultimately our ion conductivity:

$$\mu = \frac{\langle v_z \rangle}{E} \quad (2.26)$$

$$\kappa = \mu_+ \rho_{+e} + \mu_- \rho_{-e} \quad (2.27)$$

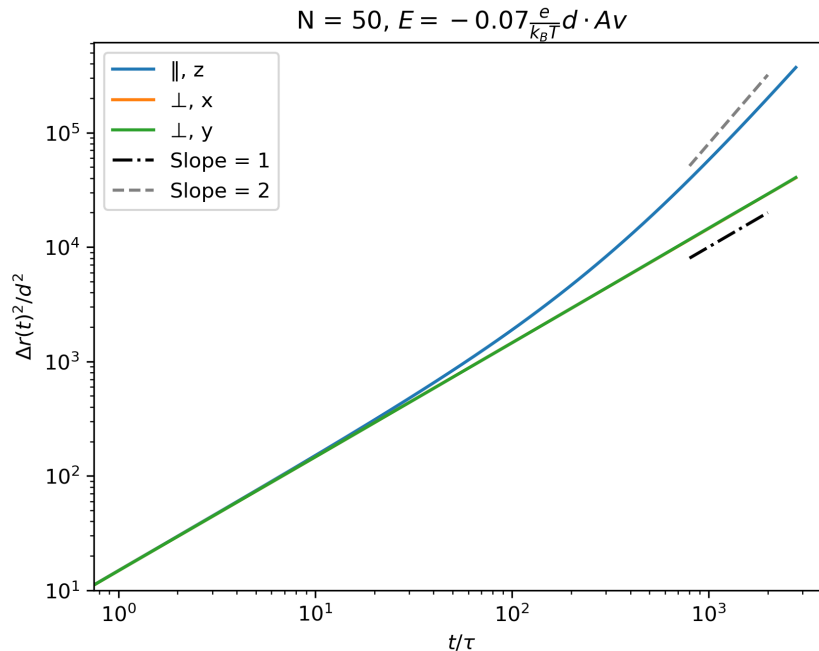


Figure 2.12: Example trajectory showing fitting data for drift velocity,  $v_z$ , extraction from applied electric field

In practice, this calculation is done by looking at the mobility,  $\mu$  response at a range of electric fields in our case (0-0.2 in reduced units). We should expect a linear response when we plot  $v_z$  against our electric field and are able to use the linear slope of that line to attain our average mobility,  $\mu$ .

Finally, we can extract the ion conductivity from the mobility using equation 2.27 to get the relationship in figure 2.14.

We get a similar trend where as chain length increases the conductivity remains relatively the same, with a maximum value around  $N = 100$ . This is an expected result given our static simulations and helps confirm our results from our equilibrium simulations - that we see a moderate increase in conductivity in very short chain length but that increase tapers off in the partially entangled regime. A quick comparison with figure 2.11, will confirm that our electric field conductivity continues to exceed our Nernst Einstein conductivity.

### 2.3 Conclusion

Our combined analysis shows that our charged PIL system obeys typical scaling laws for a polymer melt across our measured dynamic properties, with the role of electrostatics primarily influencing the magnitude of relaxation and chain size.

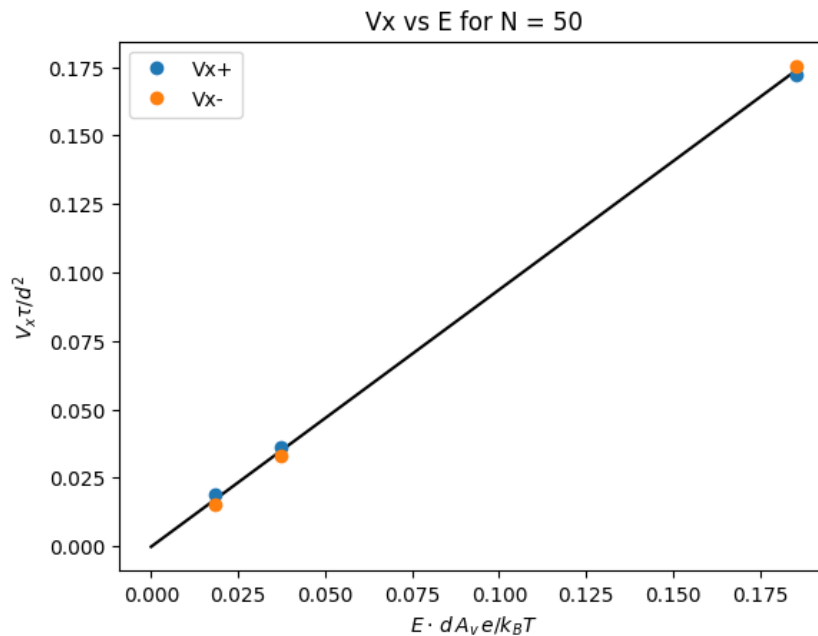


Figure 2.13: Example plot of drift velocity  $V_z$  versus electric field - notice the linear response as we increase the field strength and the clear intercept with the origin

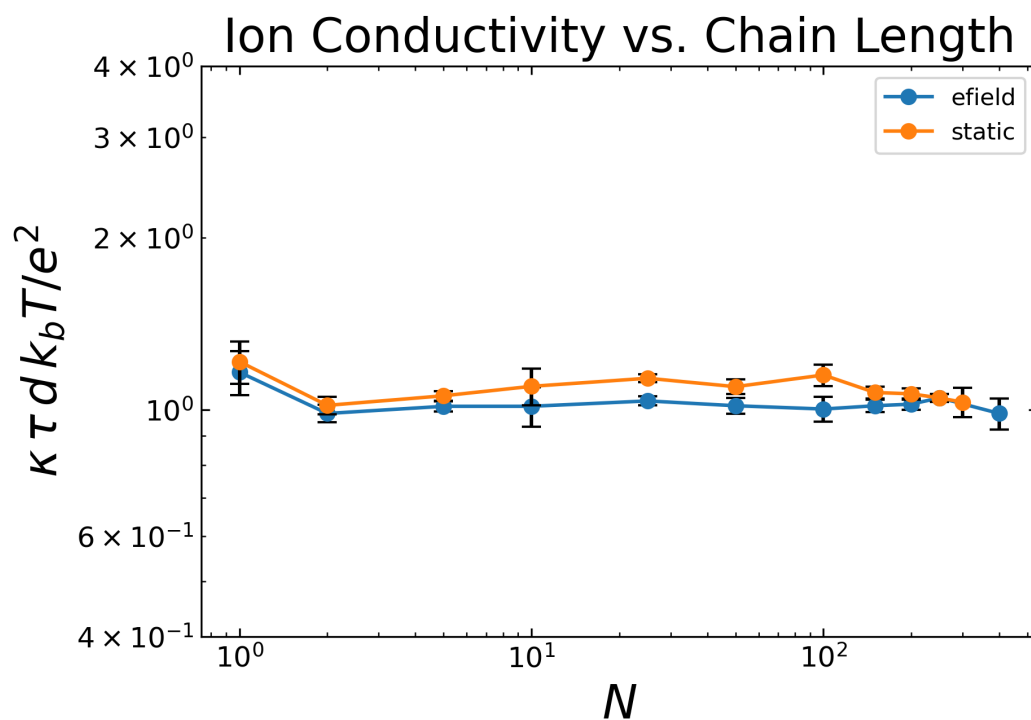


Figure 2.14: Plot of conductivity vs. chain length for applied electric field simulations

In particular, relaxation times and diffusivity adhere to the expected scaling laws even in the presence of electrostatic interactions. In the fully entangled regime, the charged polymer systems exhibit characteristic reptation scaling, again with distinctly slower time scales and larger chain size. These observations affirm that both our equilibrium and non-equilibrium measurements capture the anticipated ideality in dynamic scaling, with the charged and uncharged systems displaying closely related behavior aside from the inherent delay in relaxation and increase in chain size of the charged ensemble.

Employing the Onsager framework to investigate the correlated and anti-correlated motion of our system's ions provides a quantitative avenue to assess how electrostatic interactions shape both individual particle dynamics and collective charge transport. Our analysis reveals that in the short chain regime, the correlated motion of polyanions drives a pronounced and initial increase in ion conductivity (excluding the monomer instance). Strikingly, this initial boost gives way to a marked plateau—featuring a subtle yet persistent rise—that endures well into the semi-entangled regime before eventually tapering off fully entangled state. The slow, almost absent decline in conductivity in the fully entangled regime is an unexpected result that reflects continuing correlation between polyanions even as individual ion mobility decreases. This distinctive conductivity behavior, confirmed through both Onsager transport coefficient evaluation and direct electric field measurements, underscores the critical role of electrostatic forces in modulating polymer dynamics. This phenomenon could further inform experimental advances in these systems and emphasizes the importance of designing PILs with progressively lower glass transition temperatures to enhance ionic mobility and overall performance.

## References

1. Stukowski, A. Modelling Simul. Mater. Sci. Eng. *Modelling and Simulation in Materials Science and Engineering* **18**, 015012 (2010).
2. Eastman, P., Swails, J., Chodera, J. D., *et al.* OpenMM 7: Rapid development of high performance algorithms for molecular dynamics. *PLoS Comput. Biol.* **13** (ed Gentleman, R.) e1005659 (2017).
3. Groot, R. D. & Warren, P. B. Dissipative particle dynamics: Bridging the gap between atomistic and mesoscopic simulation. *Journal of Chemical Physics* **107**, 4423–4435 (1997).
4. Ye, B. B., Chen, S. & Wang, Z.-G. GCMe: Efficient Implementation of the Gaussian Core Model with Smeared Electrostatic Interactions for Molecular

- Dynamics Simulations of Soft Matter Systems. *Journal of Chemical Theory and Computation* **20**, 6870–6880 (2024).
5. Wang, X., Zhang, S., Yao, J. & Li, H. The Polarity of Ionic Liquids: Relationship between Relative Permittivity and Spectroscopic Parameters of Probe. *Industrial & Engineering Chemistry Research* **58**, 7352–7361 (2019).
  6. Singh, T. & Kumar, A. Static Dielectric Constant of Room Temperature Ionic Liquids: Internal Pressure and Cohesive Energy Density Approach. *The Journal of Physical Chemistry B* **112**, 12968–12972 (2008).
  7. Rubinstein, M. & Colby, R. H. *Polymer Physics* (Oxford University Press, Oxford ; New York, 2003).
  8. Hunter, J. D. Matplotlib: A 2D graphics environment. *Computing in Science & Engineering* **9**, 90–95 (2007).
  9. Hong, L. & Lei, J. Scaling law for the radius of gyration of proteins and its dependence on hydrophobicity. *Journal of Polymer Science Part B: Polymer Physics* **47**, 207–214 (2009).
  10. Elton, D. C. Stretched Exponential Relaxation. *arXiv preprint arXiv:1808.00881v1*. Published on arXiv August 3, 2018 (Aug. 2018).
  11. Fong, K. D., Self, J., McCloskey, B. D. & Persson, K. A. Ion Correlations and Their Impact on Transport in Polymer-Based Electrolytes. *Macromolecules* **54**, 2575–2591 (2021).
  12. Doi, M. *Soft Matter Physics* (Oxford University Press, Oxford, UK, 2013).
  13. Doi, M. & Edwards, S. *The Theory of Polymer Dynamics* (Clarendon Press, Oxford, 1986).
  14. Fong, K. D., Self, J., McCloskey, B. D. & Persson, K. A. Onsager Transport Coefficients and Transference Numbers in Polyelectrolyte Solutions and Polymerized Ionic Liquids. *Macromolecules* **53**, 9158–9167 (Oct. 2020).
  15. Fong, K. D., Self, J., McCloskey, B. D. & Persson, K. A. Onsager Transport Coefficients and Transference Numbers in Polyelectrolyte Solutions and Polymerized Ionic Liquids. *Macromolecules* **53**, 9503–9512 (2020).
  16. Del Pópolo, M. G., Lynden-Bell, R. M. & Kohanoff, J. Ab Initio Molecular Dynamics Simulation of a Room Temperature Ionic Liquid. *The Journal of Physical Chemistry B* **109**, 5895–5902 (2005).
  17. Bedrov, D. *et al.* Molecular Dynamics Simulations of Ionic Liquids and Electrolytes Using Polarizable Force Fields. *Chemical Reviews* **119**, 7940–7995 (2019).
  18. *Comprehensive Polymer Science and Supplements* English (eds Allen, G. & Bevington, J. C.) (Pergamon, Elsevier, Oxford, UK, 1996).

19. Fong, K. D., Bergstrom, H. K., McCloskey, B. D. & Mandadapu, K. K. Transport phenomena in electrolyte solutions: Nonequilibrium thermodynamics and statistical mechanics. *AIChE Journal* **66**, e17091 (2020).
20. Griffin, P. J. *et al.* Ion Transport in Cyclopropenium-Based Polymerized Ionic Liquids. *Macromolecules* **51**, 1681–1687 (2018).
21. Shen, K.-H. & Hall, L. M. Ion Conductivity and Correlations in Model Salt-Doped Polymers: Effects of Interaction Strength and Concentration. *Macromolecules* **53**, 3655–3668 (2020).

## Appendix A

### GAUSSIAN CORE MODEL

The Gaussian Core Model (GCMe), developed by Ben Ye [1], introduces a novel approach to coarse-grained molecular dynamics simulations that smears both electrostatics and mass across particles. This model presents two key advantages over conventional coarse-graining techniques. First, it exploits the computational acceleration afforded by modern GPU computing via an implementation in the OpenMM molecular dynamics platform [2]. Second, it employs soft-sphere particles. Traditional molecular dynamics packages, such as Kremer-Grest, struggle to accurately model densely packed ion complexes and often overestimate electrostatic forces, particularly in systems like our polymerized ionic liquids. In contrast, the soft-sphere particles used in this model can more accurately model systems of that often deform or are densely packed. Using soft-spheres also permits limited particle overlap without causing energy divergence, thereby enabling larger time steps and further enhancing computational efficiency. In total, this will allow the Gaussian Core Model to explore larger system sizes over greater time scales.

Overall, the Gaussian Core Model is exceptionally well-suited for accurately and efficiently investigating the dense ionic liquid systems analyzed in this thesis. In the subsequent sections, we will derive and parameterize the essential characteristics of the polyanion system described in Chapter 2.

#### A.1 Model and Parameterization

The coarse grained spheres in GCMe interact with one another based on their centrosymmetric pair potentials [1] where the Gaussian distributed mass density for particle  $i$  can be defined as

$$\rho_{i,m}(\mathbf{r}) = \left(\frac{3}{2\pi\sigma_i^2}\right)^{\frac{3}{2}} \exp\left(-\frac{3}{2}(\mathbf{r} - \mathbf{r}_i)^2\right) \quad (\text{A.1})$$

where  $\sigma_i$  is the mass smearing radii. While the Gaussian distributed charge density for particle  $i$  can be defined as

$$\rho_{i,q}(\mathbf{r}) = \frac{z_i e}{(2a_i^2)^{\frac{3}{2}}} \exp\left(-\frac{\pi}{2a_i}(\mathbf{r} - \mathbf{r}_i)^2\right) \quad (\text{A.2})$$

where  $a_i$  is the electrostatic smearing radii,  $z_i$  is the particle valency, and  $e$  is the elementary charge. One of the computational advantages of GCMe over other soft particle models like DPD, lies in the fact that both equations A.1 and A.2 are both analytically solvable integrals. The excluded interaction between two particles indices  $i$  and  $j$  can then be described as a gaussian interaction below

$$u_{excl}(\mathbf{r}_{ij}) = \left(\frac{3}{2\pi\sigma_{ij}^2}\right)^{\frac{3}{2}} \exp\left(-\frac{3}{2\sigma_{ij}^2}\mathbf{r}_{ij}^2\right) \quad (\text{A.3})$$

where  $\sigma_{ij}^2$  can be found from the corresponding mass smearing radii by  $\sigma_{ij}^2 = \sqrt{\sigma_i^2 + \sigma_j^2}$ ,  $r_{ij}$  is the radial distance between particles, and  $A_{ij}$  as the excluded volume scaling parameter. Similarly the smeared electrostatic interaction between two particles can be expressed as:

$$u_{elec}(\mathbf{r}_{ij}) = \left(\frac{z_i z_j e^2}{4\pi\epsilon_0\epsilon_r\mathbf{r}_{ij}}\right) \text{erf}\left(\frac{\sqrt{\pi}}{\sqrt{2}a_{ij}}\mathbf{r}_{ij}\right) \quad (\text{A.4})$$

where  $a_{ij}^2$  can be found from the corresponding mass smearing radii by  $a_{ij}^2 = \sqrt{a_i^2 + a_j^2}$ ,  $\epsilon_0$  is the permittivity of free space, and  $\epsilon_r$  is the relative permittivity (set as 12 for the systems discussed in this thesis). In order to determine appropriate values for  $A_{ij}$ , the compressibility it can be convenient to relate system pressure to simulation density. We can then use the virial theorem and the summation of the pairwise forces to make this comparison:

$$p = \rho k_b T + \frac{1}{3V} \left\langle \sum_{i < j} (\mathbf{r}_i - \mathbf{r}_j) f_i \right\rangle \quad (\text{A.5})$$

$$= \rho k_b T + \frac{2\pi}{3} \rho^2 \int_0^\infty r^3 f_{ij}(r) g_{ij}(r) dr \quad (\text{A.6})$$

In this context,  $k_b T$  represents the energy scale, while  $V$  denotes the system's volume. The variables  $f_i$  and  $r_i$  correspond to the force and position of particle  $i$ , respectively, whereas  $f_{ij}$  and  $g_{ij}$  describe the pairwise GCMe force and the radial distribution function between particles  $i$  and  $j$ . Approximating for soft spheres, where the majority contribution comes from the leading order term, we can simplify and approximate this relationship as:

$$p \approx \rho k_b T + \omega A_{ij} \rho^2 \quad (\text{A.7})$$

where  $\omega$  is a dimensionless scaling constant, derived in [1] as .499. We can then relate the dimensionless compressibility constant  $\kappa^{-1}$ , set to the value for water, 15.9835, thru a maxwell relation

$$\kappa^{-1} = \frac{1}{nk_bT\kappa_T} = \left(\frac{\partial p}{\partial \rho}\right)_T \left(\frac{\partial p}{\partial n}\right)_T \quad (\text{A.8})$$

$$= \frac{1}{N_m} \left(1 + \frac{2\omega A_{ij}\rho}{k_bT}\right) \quad (\text{A.9})$$

n here is the number density,  $\kappa_T$  is the isothermal compressibility, and  $N_m \equiv \left(\frac{\partial p}{\partial n}\right)_T$  is a size normalization factor that relates the relative size of a simulation particle to a water molecule. With these parameters, the model can be fully parameterized, and appropriate system values can be chosen. For this system we selected a  $N_m$  of 4 based on the relative dimensions of a polymerized ionic liquid monomer [3, 4], and a  $\rho$  of  $2.5 d^{-3}$  derived in [1], to appropriately represent the relative molecule size and density compared to water. The length scale,  $d$  can be defined formally as

$$d = .275nm(N_m\rho d^3)^{1/3} \quad (\text{A.10})$$

where .275 nm is the diameter of water, giving a value of  $d \approx 1.07nm$ . It then follows that individual particle size,  $\sigma = .275$  and  $.275 \text{ \AA}$  is the diameter of water. The mass of individual monomers in our system is set as  $m = m_{water}N_m \approx 72.09amu$ . The system characteristic time scale can be extracted as seen below:

$$\tau = \sqrt{\frac{md^2}{N_A k_b T}} \quad (\text{A.11})$$

Which for our  $N = 48,000$  particle polyanion and cation system is  $\approx 7.202ps$ . This is used to calculate step size,  $t = .02 \tau$ , or  $t \approx .1404$  for our studied system. With a small rearrangement, it follows then that  $A_{ij} = k_b T \frac{N_m \kappa^{-1} - 1}{2\omega\rho}$  or  $A_{ij} \approx 78.65 \frac{nm^3 kJ}{mol}$ .

## A.2 Applied Electric Field

In the instance where we apply an electric field to the polyanion system, this is done by first selecting a potential difference within the range of .1 -  $10 \frac{k_b T}{e}$  or about .25 V, well within the standard range for ionic liquids [5, 6]. The voltage is then scaled by both the system energy and size as seen below:

$$E = -V \frac{k_b T N_a}{e d} \quad (\text{A.12})$$

where  $E$  is the applied electric field,  $V$  is the thermal voltage difference,  $e$  is the elementary charge, and  $N_a$  is Avogadro's number. For a  $V$  of 1,

$$E \approx -0.04323, \frac{\text{kJ}}{\text{nm} \cdot \text{mol} \cdot e}$$

. Then a force is applied to all charged particles in the system based on their charge.

$$f_i = q_i E \quad (\text{A.13})$$

Here,  $f_i$  is the force applied to particle  $i$  and  $q_i$  is the charge on particle  $i$ , or +1 or -1 for each polyanion or cation bead. Since the applied electric field is negative, or  $E < 0$ , positive ions in our system ( $q_i > 0$ ) will have a negative force. In practice this means that positive ions will move with the field in the negative direction and negative ions will move in the positive direction. See below graphic for clarity:

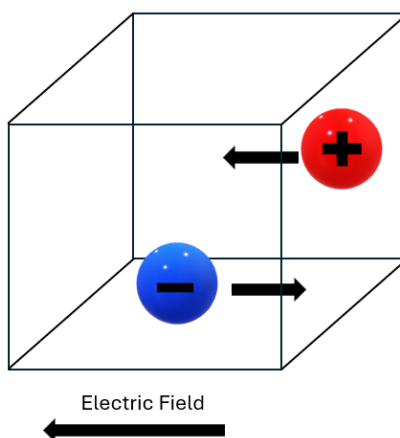


Figure A.1: Electric field graphic

### A.3 Conclusion

This methodology combined with the GPU enabled OpenMM platform represents a powerful way to explore systems that benefit from soft sphere, and require large systems studied at relatively long time frames. This appendix reviews the implementation and employment of key model parameters that are underlying the simulations in this thesis.

### References

1. Ye, B. B., Chen, S. & Wang, Z.-G. GCMe: Efficient Implementation of the Gaussian Core Model with Smeared Electrostatic Interactions for Molecular Dynamics Simulations of Soft Matter Systems. *Journal of Chemical Theory and Computation* **20**, 6870–6880 (2024).
2. Eastman, P., Swails, J., Chodera, J. D., *et al.* OpenMM 7: Rapid development of high performance algorithms for molecular dynamics. *PLoS Comput. Biol.* **13** (ed Gentleman, R.) e1005659 (2017).

3. Liu, G., Luo, H., Dan, Y., Niu, Y. & Li, G. Scaling Relation and Rheological Behaviors of Polymerized Ionic Liquids in Ionic Liquid/Dimethylformamide Solutions. *Macromolecules* **57**, 8409–8420 (2024).
4. Matsumoto, A. & Shen, A. Q. Rheological scaling of ionic-liquid-based polyelectrolytes in ionic liquid solutions: the effect of the ion diameter of ionic liquids. *Soft Matter* **18**, 4197–4204 (2022).
5. Wang, Y. *et al.* Tuning of Ionic Liquid–Solvent Electrolytes for High-Voltage Electrochemical Double Layer Capacitors: A Review. *Batteries* **10**, 54 (2024).
6. Manna, S. S., Bhauriyal, P. & Pathak, B. Identifying suitable ionic liquid electrolytes for Al dual-ion batteries: role of electrochemical window, conductivity and voltage. *Mater. Adv.* **1**, 1354 (2020).

## *Appendix B*

### ONSAGER TRANSPORT COEFFICIENT FITTING

In this appendix we will describe and show how Onsager transport coefficients, and other key values were extracted from simulation trajectories. The point here is to show clearly how these quantities were fitted, substantiate the values represented in this thesis, and to serve as a support for analytical methods of Chapter 2 of this thesis.

#### **B.1 Mean Squared Displacement and Diffusivity**

Diffusivity measurements, used in the dynamics scaling law relationship, were taken using the middle 20% monomers from each polyanion. This was done to replicate the center of mass diffusivity while keeping a statistically significant amount of data points in systems with limited total chains; for example for  $N = 300$  system, with a system size of 96,000 particles, equating to 160 total chains. Again, the mean squared displacement was calculated using equation 2.8, using the ensemble average of each individual particle squared displacement. For a relaxing polymer obeying the reptation model, like in one of the equilibrium simulations, we expect that polymer to mean squared displacement after a ballistic region to initially scale with  $t^{1/2}$  and then transition into a diffusive regime where it scales with  $t^1$  [1].

Additionally, when looking at our uncharged systems it is important to note that they undergo a similar initial scaling of  $t^{1/2}$  and then transitioning into a diffusive regime where it scales with  $t^1$  at sufficiently long time. The key difference between figure ?? is the much quicker transition to the diffusive regime, and greater magnitude of displacement.

For short chain polymers, this transition region within the time scale we are studying can be very small, but in long chained polymer, this region can be more pronounced, see figure B.1. The mean square displacement for these trajectories are then fitted from their diffusive region, where the MSD scales with  $t^1$ , or where their slope in the log-log space is one. Using that fit data, we are able to generate figure 2.5. Looking at a range of chain lengths we can see the expected trend where displacement decreases as chain length increases, in figure B.3.

Note in figure B.3, that cations are immediately diffusive, and relatively close values

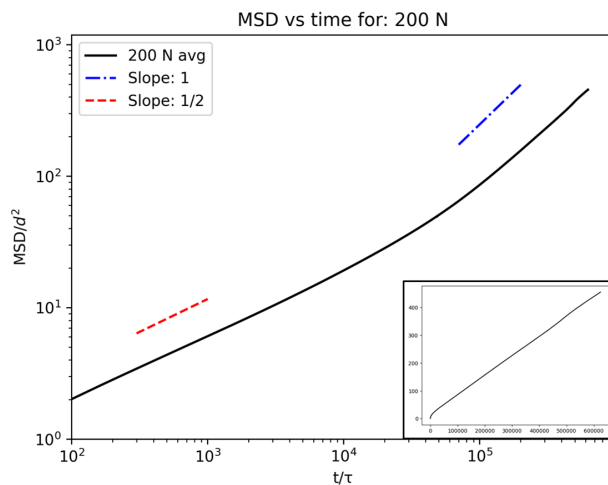


Figure B.1: Example log-log mean squared displacement of charged polyanion system where diffusive slope = 1. Also displayed is linear scale of the same trajectory.

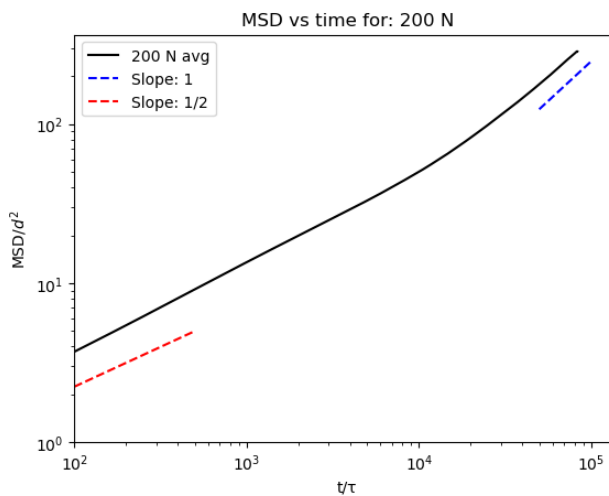


Figure B.2: Example log-log mean squared displacement of uncharged polymer system where diffusive slope = 1. Note comparatively short time scale to enter diffusive regime when compared to polyanion system.

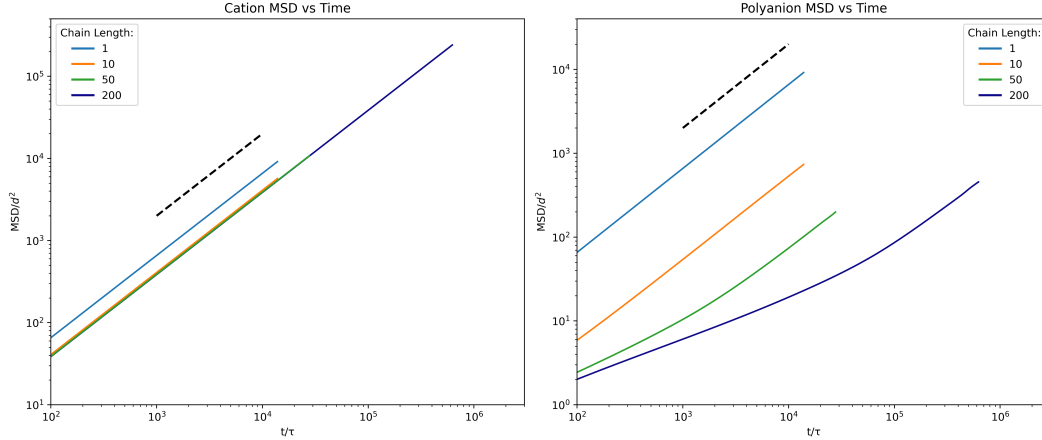


Figure B.3: Mean squared displacement, for cation and polyanions in our static system, varied over chain length. Diffusivity values were fit from the diffusive regime, where the log-log slope is 1 (dashed line).

correspond to asymptotic behavior in  $L_{++}^{self}$  in 2.7. While the substantial difference in polyanion displacement is borne out in  $L_{--}^{self}$  the same figure and the polymer diffusivity (figure 2.5)

## B.2 Onsager Coefficient

The Onsager Coefficients are similarly fitted from the analog to mean squared displacement for each of the corresponding summations (see equations 2.17, 2.14) [2]. As equation 2.20 implies, the self terms for both  $L_{--}^{self}$  and  $L_{++}^{self}$  can be fitted directly from the mean squared displacements as seen in figure B.3. Again, this is done by fitting data from the diffusive regime for each trajectory.

For the full and distinct components of the Onsager transport coefficients, we use a modified form of the mean squared displacement, referred to as "MSD". This is done plotting the summation components of equation 2.14 - stated explicitly, we are plotting:

$$'MSD' = \left\langle \sum_{\alpha} \sum_{\beta} [\mathbf{r}_{i,\alpha}(t) - \mathbf{r}_{i,\alpha}(0)] \cdot [\mathbf{r}_{i,\beta}(t) - \mathbf{r}_{i,\beta}(0)] \right\rangle \quad (\text{B.1})$$

Then, as described in Chapter 2, to recover the  $L_{++}^{distinct}$  and  $L_{--}^{distinct}$  terms we can add back in the self components (eg.  $L_{++} = L_{++}^{self} + L_{++}^{distinct}$ ). Note, because there remains a self component in the cross term (eg. the self portion of the dot product remains inside the summation),  $L_{+-}$  can be extracted directly from the 'MSD', without an additional summation. Additionally, because the  $L_{+-}$  is negative, the

absolute value of the trajectory is used to extract the Onsager transport coefficient in the log-log space. An example of this can be seen below in figure B.4:

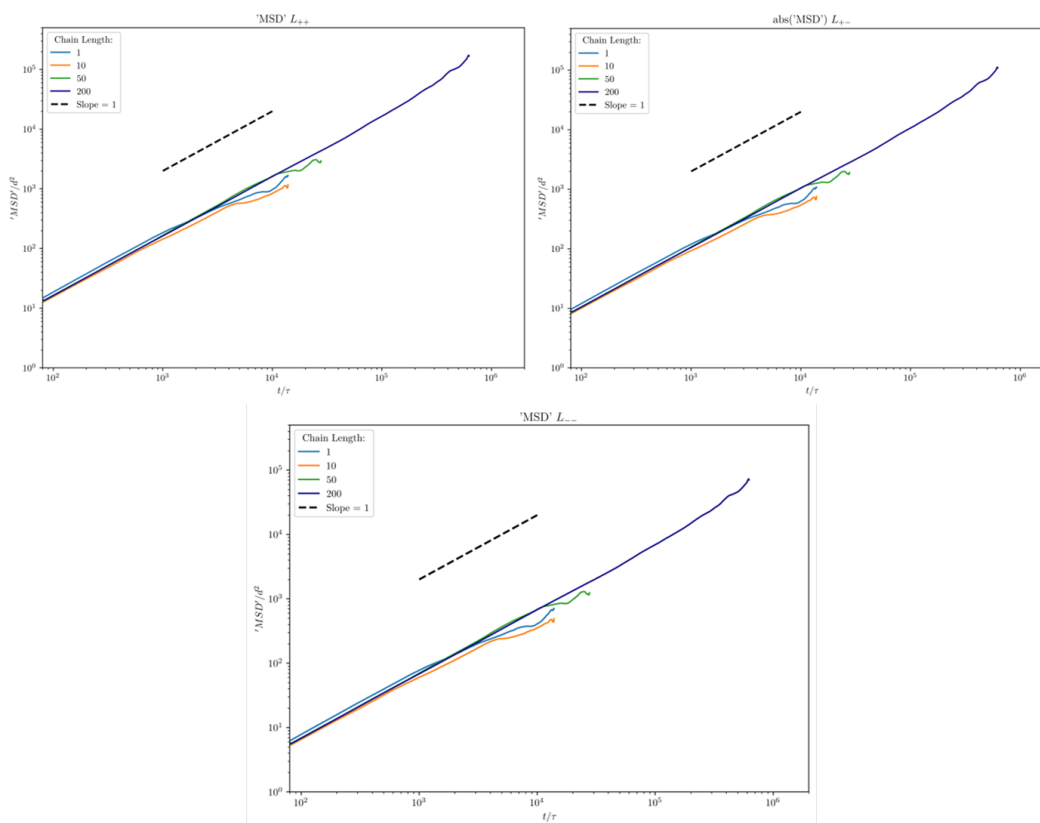


Figure B.4: "MSD" terms for the full  $L_{ij}$  terms in the Onsager transport coefficient framework that were used to fit data with a reference slope of 1. Note, longer chained trajectories were run for longer periods of time to achieve full relaxation and ensure trajectories are in the diffusive regime.

## References

1. Rubinstein, M. & Colby, R. H. *Polymer Physics* (Oxford University Press, Oxford ; New York, 2003).
2. Fong, K. D., Self, J., McCloskey, B. D. & Persson, K. A. Onsager Transport Coefficients and Transference Numbers in Polyelectrolyte Solutions and Polymerized Ionic Liquids. *Macromolecules* **53**, 9158–9167 (Oct. 2020).